RSC Advances

PAPER

View Article Online
View Journal | View Issue

Cite this: *RSC Adv.*, 2024, **14**, 8353

Fabrication of a surface molecularly imprinted polymer membrane based on a single template and its application in the separation and extraction of phenytoin, phenobarbital and lamotrigine†

Yan-lin Zhao,‡[a] Yu-xin You,‡[b] Yu-lang Chen,[a] Ying Zhang,[a] Yan Du[bc] and Dao-quan Tang *[ab]

An innovative molecularly imprinted polymer membrane (MIPM) was prepared with polyvinylidene difluoride (PVDF) as the support, phenytoin (PHT) as the single template, methacrylic acid as the functional monomer, ethylene glycol dimethacrylate as the cross-linking reagent, azobisisobutyronitrile as the initiator, and acetonitrile–dimethylformamide (1 : 1.5, v/v) as the porogen. These materials were characterized *via* scanning electron microscopy, Fourier transform infrared spectroscopy, Brunauer–Emmett–Teller measurements and X-ray photoelectron spectroscopy. Their adsorption performances were evaluated through a series of experiments including isothermal adsorption, kinetic adsorption, selective adsorption, adsorption–desorption, reusability, and preparation reproducibility. Additionally, the application was explored by investigating the extraction recovery of MIPMs towards PHT, phenobarbital (PHB) and lamotrigine (LTG) in different matrices including methanol, normal saline (NS), phosphate buffer solution (PBS) and plasma. The results showed that MIPMs with rough and porous surfaces were successfully constructed, which offered good preparation reproducibility, reusability and selectivity. The adsorption capacities of MIPMs towards PHT, PHB and LTG were 2.312, 2.485 and 2.303 mg g^{-1}, respectively, while their corresponding imprinting factors were 8.538, 12.122 and 4.562, respectively. The adsorption equilibrium of MIPMs was achieved within 20 min at room temperature without stirring or ultrasonication. The extraction recoveries of MIPMs for PHT, PHB or LTG in methanol, NS and PBS were more than 80% with an RSD% value of less than 3.64. In the case of plasma, the extraction recovery of MIPMs for PHT and PHB was more than 80% with an RSD% value of less than 2.41, while that of MIPMs for LTG was more than 65% with an RSD% value of less than 0.99. All the results indicated that the preparation method for MIPMs was simple, stable, and reliable, and the prepared MIPMs possessed excellent properties to meet the extraction application of PHT, PHB and LTG in different matrices.

Received 11th January 2024
Accepted 19th February 2024

DOI: 10.1039/d4ra00294f

rsc.li/rsc-advances

1. Introduction

Epilepsy is a type of central nervous system disease characterized by sudden abnormal discharge of neurons and has become the second most-common neurological disorder followed by headaches.[1,2] At present, pharmacological treatment with antiepileptic drugs (AEDs) is the primary choice for most patients with epilepsy. However, the inter-individual variability of drug concentration in epileptic patients treated with AEDs may result in inter-individual therapeutic efficacy and adverse/toxic effects.[3] Thus, monitoring the blood concentration of AEDs is commonly required to optimize their individual dose, improve their therapeutic efficacy, and decrease their adverse and toxic effects in the clinical management of patients with epilepsy.[4]

Phenytoin (PHT) and phenobarbital (PHB) are the first-generation AEDs used in the treatment of epilepsy. However, although they present obvious inter-individual variability, narrow therapeutic scopes, nonlinear pharmacokinetics and serious adverse effects, they are still widely used in the treatment of focal, generalized and neonatal seizures owing to their broad spectrum treatment range and low cost.[5–7] Lamotrigine (LTG) is another broad spectrum AED used for the treatment of

[a]*Department of Pharmacy, Suining People's Hospital Affiliated to Xuzhou Medical University, Suining 221202, China*

[b]*Jiangsu Key Laboratory of New Drug Research and Clinical Pharmacy, Xuzhou Medical University, 209 Tongshan Road, Xuzhou 221004, Jiangsu Province, China. E-mail: tdq993@hotmail.com; tangdq@xzhmu.edu.cn; Fax: +86 516 83263313; Tel: +86 516 83263313*

[c]*State Key Laboratory of Pharmaceutical Biotechnology, Chemistry and Biomedicine Innovation Center (ChemBIC), Jiangsu Key Laboratory of Molecular Medicine, Medical School, Nanjing University, Nanjing, 210093, China*

† Electronic supplementary information (ESI) available. See DOI: https://doi.org/10.1039/d4ra00294f

‡ These authors contributed to the work equally and should be regarded as co-first authors.

focal and generalized seizures and is commonly the first choice of drug in the treatment of multiple types of seizures or undefined types of seizures.[8] As a second-generation AED, LTG has overcome the disadvantages of first-generation AEDs. However, serious side effects may occur during treatment with LTG because of a large inter-individual variability influenced by unpredictable pharmacokinetic interaction from drug–drug or drug–food.[9,10] Thus, monitoring the blood concentration of PHT, PHB and LTG is important for their rational clinical application.

Additionally, the potential threat to the ecological environment from organic micropollutants in environmental water from pharmaceuticals has attracted comprehensive attention and become a worldwide environmental concern.[11] Residue of PHT, PHB or LTG in industrial or municipal wastewater may enter the environmental water, and thus pose a threat to ecological safety.[12–14] For example, Cardoso-Vera's group demonstrated that an environmentally relevant concentration of PHT may induce oxidative stress in zebrafish embryos and brains of adult zebrafish, and increase the acetylcholinesterase level in adult zebrafish, thus affecting the embryonic development of zebrafish or triggering a harmful response in the brain of adult zebrafish.[15,16] Another report showed that PHT and LTG in treated wastewater may induce a stress response in tomato plants.[17] Unchanged forms of PHB excreted through the kidney can contribute to aquatic contamination and potential damage to human health and the environment.[18,19] Sörengård's study indicated that LTG presented the highest risk quotient values for *Daphnia* and fish.[20] Goldstein *et al.* speculated that environmental pH may produce ionized LTG, which may bind to the negatively charged plant cell wall, and thus hinder its translocation in the plant.[21] As mentioned above, the environmental risk of PHT, PHB or LTG necessitates their monitoring and improvement of environmental water treatment and management.

High-performance liquid chromatography (HPLC) coupled with spectrometry has become an important technique for the monitoring of PHT, PHB or LTG in environmental water, urine, and plasma.[17,22,23] During this process, the extraction and separation of PHT, PHB or LTG from matrices is the first and key step. Recently, solid-phase extraction (SPE) based on molecularly imprinted polymers has aroused comprehensive attention from scientists in the fields of environmental and biomedical analysis,[24–26] which has been successfully applied in the determination of PHT, PHB or LTG in environmental water, urine, serum, and plasma.[27–33] Compared with the traditional SPE column, molecularly imprinted polymer membranes (MIPMs) have received more extensive attention for the separation and extraction of target compounds in biological samples or environmental water, given that they simultaneously possess the advantages of molecularly imprinting and membrane technology, such as specific recognition, specific surface area, and convenient operation.[34–38] However, to the best of our knowledge, MIPMs suitable for the targeted extraction and separation of PHT, PHB, and/or LTG in different matrices have not been reported to date.

In the current study, based on surface imprinting and free radical polymerization, a novel MIPM using PHT as the single template and polyvinylidene difluoride (PVDF) membrane as the support was successfully designed, optimized and prepared. The usability of MIPMs was evaluated by combining MIPM extraction and HPLC for the determination of PHT, PHB, and LTG in different matrices such as methanol, normal saline (NS), phosphate buffer solution (PBS), and plasma. The proposed method showed an excellent adsorption performance for PHT, PHB, and LTG, which may broaden the application of MIPMs in different chemical separations. The research findings in this study possess obvious scientific significance and present a great potential in practical applications.

2. Materials and methods

2.1. Reagents and materials

PHB was a gift from Xuzhou Municipal Hospital (Xuzhou First People's Hospital). The reference PHT (Batch No. C11997231), oxcarbazepine (OXC, Batch No. C11956913), LTG (Batch No. C14769829), and carbamazepine (CBZ, Batch No. C11880371) were purchased from Macklin Biochemical Technology Co., Ltd. (Shanghai China), while 2,2-diphenylglycine (DPG, Batch No. H2206795) was provided by Aladdin Biochemical Technology Co., Ltd. (Shanghai, China), and their purities were guaranteed to be more than 98% by the producers. Chromatographic grade acetonitrile (ACN) and methanol were obtained from Thermo Fisher Scientific (Waltham, MA, USA), while potassium dihydrogen phosphate (Batch No. A2114155, ≥99.9%) was purchased from Aladdin Biochemical Technology Co., Ltd. (Shanghai, China). Analytical grade methacrylic acid (MAA, Batch No. C10649624, ≥99.9%) and azobisisobutyronitrile (AIBN, Batch No. B040239, ≥98.0%) were provided by Macklin (Shanghai China) and Energy Chemical (Shanghai, China), respectively, while ethylene glycol dimethacrylate (EGDMA, Batch No. I2001232, ≥98.0%), 4-vinylbenzoic acid (VBA, Batch No. G2017034, ≥97.0%), methyl methacrylate (MMA, Batch No. L2106692, ≥99.5%), trimethylolpropane trimethacrylate (TRIM, Batch No. K1915182, ≥98.0%), methacrylamide (MAAm, Batch No. C10686192, ≥98.0%), acrylamide (AM, Batch No. E2107071, ≥99.9%), and *N*,*N*-dimethylformamide (DMF, Batch No. C2118167, ≥99.9%) were purchased from Aladdin Biochemical Technology Co., Ltd. (Shanghai, China). Analytical grade methanol (Batch No. 20210810), ethanol (Batch No. 20220113) and acetic acid (Batch No. 20210118) were purchased from Sinopharm Chemical Reagent Co. Ltd. (Shanghai China). Commercially available PVDF membrane was purchased from Merk Co. Ltd. (Darmstadt, Germany), while Nylon 66 (NY-66), polypropylene (PP), and polytetrafluoroethylene (PTFE) membranes were obtained from Haining Zhongli Filtering Equipment Factory (Haining, Zhejiang, China).

2.2. Fabrication of PHT-MIPMs

The process for the preparation of MIPMs is illustrated in Fig. 1. In detail, PVDF membranes were firstly cut in a square shape (2 cm × 2 cm) and activated by immersion in methanol for 24 h,

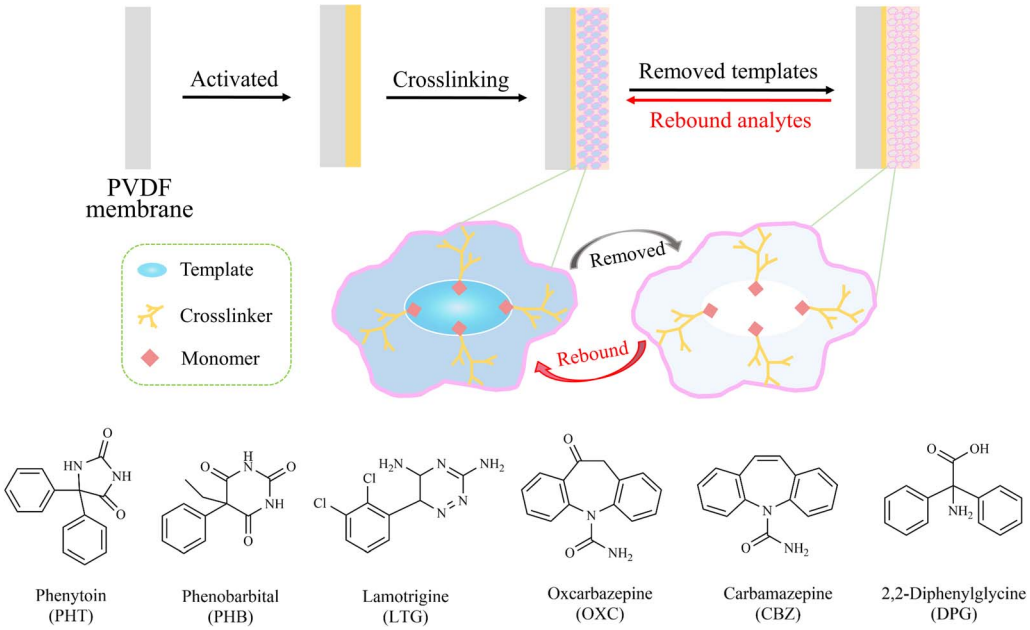

Fig. 1 Schematic diagram for the preparation of molecularly imprinted polymer membranes (MIPMs) toward phenytoin, phenobarbital, and lamotrigine, and the chemical structures of compounds used in current study.

washing with distilled water 3 times, and then immersion in 0.05 mol L^{-1} AIBN methanol solution for 10 min. The activated PVDF membranes were dried at ambient temperature for future use. The pre-polymerization solution was obtained by mixing 55.97 mg of PHT (0.2 mmol), 522 μL of MMA (6.0 mmol), and 2.5 mL of ACN–DMF (1 : 1.5, v/v) under ultrasonication for 10 min at room temperature. Then, 16.76 mg of AIBN (0.1 mmol), 809 μL of EGDMA (4.0 mmol), and the activated PVDF membrane were placed in a pre-polymerization solution. The mixture was reacted for 25 min at ambient temperature with nitrogen, and then 24 h in 60 °C an oil bath. Finally, PHT-MIPMs were obtained after drying at room temperature and removing the template by washing with methanol–acetic acid (9 : 1, v/v) and methanol in sequence. Similarly, non-imprinted polymer membranes (NIPMs) were simultaneously prepared using the same method as above without the addition of PHT.

2.3. Characterization of materials

The surface morphology, functional groups, surface areas and elemental analysis of PVDF, MIPMs and NIPMs were characterized by scanning electron microscopy (SEM) (QUANTA FEG 450, FEI, USA), Fourier transform infrared spectroscopy (FT-IR 360, Shimadzu, Japan), surface area analysis (ASAP2460, Micromeritics, USA) using the Brunauer–Emmet–Teller (BET) method, and X-ray photoelectron spectroscopy (XPS) (ESCALAB 250Xi, Thermo Fisher Scientific, USA), respectively.

2.4. Evaluation of the adsorption performance of the materials

The adsorption performance of MIPMs or NIPMs was evaluated by static adsorption, kinetic adsorption, selective adsorption, adsorption–desorption, and reusability and reproducibility experiments. Analytes in residual solution or desorption solution were determined by HPLC-UV and the chromatographic conditions are presented in the ESI.†

2.4.1. Static adsorption. MIPMs or NIPMs were placed in 5 mL methanol solution containing PHT, PHB or LTG at the concentrations of 10, 20, 30, 40, 60, 80, 100, or 150 μg mL^{-1} for 2 h of static adsorption at ambient temperature, respectively. Then, the residual solution was filtered with a 0.22 μm nylon membrane and determined by HPLC-UV after MIPMs or NIPMs were taken out. The adsorption capacity was calculated according to eqn (1), and the isotherm adsorption models including linearized Langmuir chemical adsorption, non-linearized Freundlich physical adsorption, and Dubinin–Radushkevich based on Polanyi's potential theory were fitted according to eqn (2)–(4), as follows:[30,39]

$$Q_e = \frac{(C_0 - C_e)V}{W} \quad (1)$$

where Q_e, C_0, C_e, V, and W are the adsorption capacity (mg g^{-1}), initial solution concentration (μg mL^{-1}), solution concentration after adsorption equilibrium (μg mL^{-1}), adsorption solution volume (mL), and dry weight of MIPMs or NIPMs (mg), respectively.

$$\frac{C_e}{Q_e} = \frac{1}{KQ_m} + \frac{C_e}{Q_m} \quad (2)$$

where Q_m is the maximum adsorption capacity (mg g^{-1}) and K is the Langmuir model constant.

$$\ln Q_e = \ln K_F + \frac{1}{n}\ln C_e \quad (3)$$

where K_F is the Freundlich model constant (mg g^{-1}) and n is the adsorption intensity parameter.

$$\ln Q_e = \ln Q_m - k_{ad}\varepsilon^2 \quad (4)$$

where k_{ad} (mol^2 J^{-2}) is the adsorption free energy activity coefficient and ε is the Polanyi adsorption potential and calculated by $RT\ln(1 + 1/C_e)$, in which T is the absolute temperature and R (8.314 J mol^{-1} K^{-1}) is the gas constant.

2.4.2. Kinetic adsorption. MIPMs or NIPMs were immersed in 5 mL of 80 μg mL^{-1} PHT, PHB or LTG methanol solution and statically placed at ambient temperature. The residual solution was sampled at 2, 5, 10, 15, 20, 30, 40, 60, 90 or 120 min, respectively, filtered using a 0.22 μm nylon membrane, and then determined by HPLC-UV. The adsorption capacity was calculated using eqn (1) and the adsorption kinetics was fitted by the pseudo-first-order rate and pseudo-second-order rate using eqn (5) and (6), as follows:[30]

$$\ln(Q_e - Q_t) = \ln Q_e - \frac{k_1 t}{2.303} \quad (5)$$

$$\frac{t}{Q_t} = \frac{1}{k_2 Q_e^2} + \frac{t}{Q_e} \quad (6)$$

where Q_t (mg g^{-1}) is the adsorption capacity at adsorption time t (min) and k_1 and k_2 are the corresponding pseudo-first-order and pseudo-second-order adsorption rate constants, respectively.

2.4.3. Adsorption selectivity. MIPMs or NIPMs were put in 5 mL methanol solution containing PHT, PHB, LTG, DPG, OXC or CBZ at the concentration of 80 μg mL^{-1} for 2 h of standing time at ambient temperature. The structures of these compounds are presented in Fig. 1. Then, the residual solution was sampled, filtered using a 2.2 μm nylon membrane, and then determined by HPLC-UV. The adsorption capacity (Q_e), distribution coefficient (K_d), selection coefficient (α), and relative selectivity coefficient (β) were calculated using eqn (1), (7), (8) and (9), respectively, as follows:[30]

$$K_d = Q_e/C_e \quad (7)$$

$$\alpha = K_{d(template)}/K_{d(interferent)} \quad (8)$$

$$\beta = \alpha_{(MIPMs)}/\alpha_{(NIPMs)} \quad (9)$$

2.4.4. Adsorption–desorption. MIPMs were placed in 5 mL solution containing PHT, PHB or LTG at the concentration of 80 μg mL^{-1} for 20 min of static adsorption at ambient temperature. Subsequently, the adsorption-saturated MIPMs were taken out and the concentration of residual solution was determined to calculate their adsorption capacity (Q_e). Then the MIPMs were immersed in desorption reagent for 5, 10, 20, 30, 40, and 60 min at ambient temperature and the analytes in the desorption reagent were quantified by HPLC-UV to calculate the desorption capacity (Q_d). The desorption rate ($Q_d/Q_e \times 100\%$) was calculated and used as an index to evaluate the adsorption–desorption of MIPMs for the optimization of the desorption reagents.

2.4.5. Preparation reproducibility and reusability experiments. 5 batches of PHT-MIPMs were prepared with 3 replicates under the optimum conditions and the adsorption–desorption test was performed. The variation in the adsorption capacity of MIPMs was employed to evaluate their preparation reproducibility. The reusability of MIPMs was assessed by the variation in their adsorption capacity with 8 adsorption–desorption cycles.

2.5. Usability evaluation of MIPMs

In this part, PHT, PHB, or LTG reference solution at the concentration of 3 levels was spiked in methanol, NS, PBS, and rat blank plasma to simulate the practical chemical industry samples, environmental water, urine, and plasma, respectively.[40,41] Extraction experiments of the target analytes in different matrices were carried out to investigate the practical application of MIPMs. It was noted that in this study, the plasma sample needed to be diluted by 4 times with PBS before treatment with MIPMs, while the other matrices sample could be treated with MIPMs directly. After static adsorption for 20 min, the eluent of MIPMs was determined by HPLC and the extraction recovery of the target compounds was calculated to appraise the usability. In addition, for plasma, the matrix interference and extraction recovery of MIPMs towards the target compounds were also evaluated by comparing with ACN protein precipitation. Rat blank plasma and urine were a gift from the Laboratory Animals of Xuzhou Medical University, and all animal procedures were performed in accordance with the Guidelines for Care and Use of Laboratory Animals of Xuzhou Medical University and approved by the Animal Ethics Committee of Xuzhou Medical University (No. 201902A031).

HPLC analysis of PHT, PHB, or LTG in this experiment was carried out on a Waters Alliance HPLC system consisting of Waters 2695 Separations Module connected to a Waters 2998 PDA Absorbance Detector. Sample separation was performed on an Agilent Zorbax SB-C18 column (150 mm × 4.6 mm, 5 μm) kept at 35 °C. The mobile phase consisted of ACN (A) and 10 mM potassium dihydrogen phosphate water solution (B) at the flow of 1.0 mL min^{-1}. The optimal gradient elution program was set as follows: 0.0–1.0 min, 90% B; 1.0–1.5 min, 55–90% B; 1.5–7.5 min, 55% B; 7.5–8.0 min, 55–90% B; 8.0–10.0 min, 90% B. The auto-sampler temperature was maintained at 4 °C and the injection volume was 10 μL. The detection wavelength was set at 210 nm.

3. Results and discussion

3.1. Preparation of PHT-MIPMs

To achieve MIPMs with the optimal adsorption performance, some experimental parameters, such as type and amount of supporting membrane, template, functional monomer, crossing-linking agent and initiator, were optimized. These factors playing critical roles in both the synthesis and adsorption capacity of MIPMs were optimized by a single factor experiment. For the selection of a single template, given that the chemical structure of PHB is similar to that of LTG, while the chemical structure of PHT is different from that of PHB or LTG (Fig. 1), this study observed the influence of PHT and LTG on the absorption capacities of MIMPs. The detailed experimental

parameters are presented in Tables S1–S9† and the HPLC conditions used to detect PHT in the residual solution are listed in the ESI.†

According to the results presented in Fig. S1,† MIPMs exhibited superior adsorption capacity when they were synthesized using PVDF as the supporting membrane, 0.20 mmol PHT as the template, MMA as the functional monomer, and EGDMA as the cross-linking agent. The optimal molar ratio of template/functional monomer/cross-linking agent was found to be 1 : 30 : 20. Meanwhile, 0.10 mmol of AIBN served as the initiator and 2.25 mL of ACN–DMF mixture (1 : 1.5, v/v) was employed as the porogen.

3.2. Characterization of materials

In our current study, MIPMs and NIPMs were characterized by SEM, FT-IR, XPS, and BET. As shown in Fig. 2, compared with PVDF with lots of irregular cavities, NIPM had a rough and dense stack layer on its surface, which was associated with the cross-linking of the molecularly imprinted polymer on the membrane. After the templates were washed and removed, a porous structure was presented on the surface of MIPM for the identification of the target analytes.

The FT-IR spectrum of NIPM and MIPM, using the PVDF membrane as the control, are presented in Fig. 3A. The stretching vibration peaks for the functional groups C=O at approximately 1721 cm^{-1} and C=C at approximately 1659 cm^{-1} can be attributed to MMA and EGDMA, suggesting the existence of molecularly printed polymers grafted on the surface of PVDF membrane. PVDF contains carbon (C), hydrogen (H) and fluorine (F) elements, while PHT contains C, H, oxygen (O) and nitrogen (N) elements. The XPS results presented the corresponding information for the elements in present in PVDF and PHT (Fig. 3B). On the one hand, the appearance of an O 1s characteristic peak in NIPMs, MIPMs, and MIPMs with template further clarified that the molecularly imprinted polymers were successfully grafted to the surface of PVDF. On the other hand, the characteristic peak of N 1s at the binding energy 408 eV was presented both in PHT-MIPMs with templates and PHT but not in NIPMs and MIPMs, which indicated that the templates were successfully removed from MIPMs by washing, and NIPMs did not contain PHT. The surface area and porosity were investigated by nitrogen adsorption–desorption isotherms, and the pore size distribution curves are presented in Fig. 3C and D, respectively. MIPMs and NIPMs exhibited clear type IV hysteresis loops and a relatively concentrated aperture distribution, further identifying their porous structure, which was mainly mesoporous. According to the BET data listed in Table 1, MIPMs appeared to have bigger superficial area and pore size than NIPMs, indicating that more cavities were formed in MIPMs after the templates were washed out. The above-mentioned results indicate that MIPMs were successfully prepared and had a porous structure for analyte recognition.

3.3. Adsorption performance evaluation of MIPMs

The adsorption properties of MIPMs were evaluated through isothermal adsorption, dynamic adsorption, selective adsorption and adsorption–desorption. HPLC-UV was used to determine the target compounds in the residual solution, and the representative HPLC-UV chromatograms of PHT, PHB, LTG, DPG, OXC and CBZ are shown in Fig. S2.†

3.3.1. Static and kinetic adsorption. The isothermal adsorption curves, Langmuir chemical adsorption model, non-linearized Freundlich physical adsorption model, and Dubinin–Radushkevich model based on Polanyi's potential theory for MIPMs and NIPMs towards PHT, PHB, and LTG are presented in Fig. 4. The parameters of the Langmuir, Freundlich, and Dubinin–Radushkevich models are listed in Table 2. As illustrated in Fig. 4A, E, and I, the adsorption capacities of MIPMs towards PHT, PHB, and LTG increased with an increasing concentration in the range of 10–60 μg mL^{-1}, 10–80 μg mL^{-1}, and 10–40 μg mL^{-1}, respectively, and then flattened. The maximum adsorption capacities of MIPMs towards PHT, PHB, and LTG were 2.312, 2.485, and 2.303 mg g^{-1}, respectively. The adsorption capacities of NIPMs towards PHT, PHB, and LTG increased with an increasing concentration in the range of 10–40 μg mL^{-1}; however, the increased slopes were lower than that of MIPMs. Moreover, the adsorption capacities of NIPMs towards PHT, PHB, and LTG at the corresponding concentrations were all much lower than that of MIPMs. As shown in Fig. 4B–D, F–H, J–L, and Table 2, the R^2 values of PHT, PHB, and LTG in the Langmuir model were 0.9945, 0.9857, and 0.9903, respectively, which are higher than that in Freundlich or Dubinin–Radushkevich models. The results indicate that the Langmuir model well fitted the static adsorption of PHT, PHB,

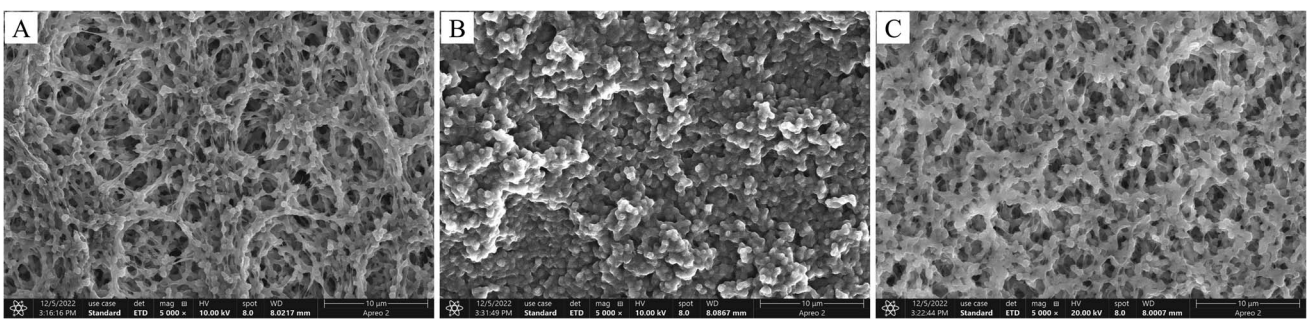

Fig. 2 Representative scanning electron microscopy images (A–C) of PVDF, non-molecularly imprinted polymer membranes (NIPMs), and MIPMs.

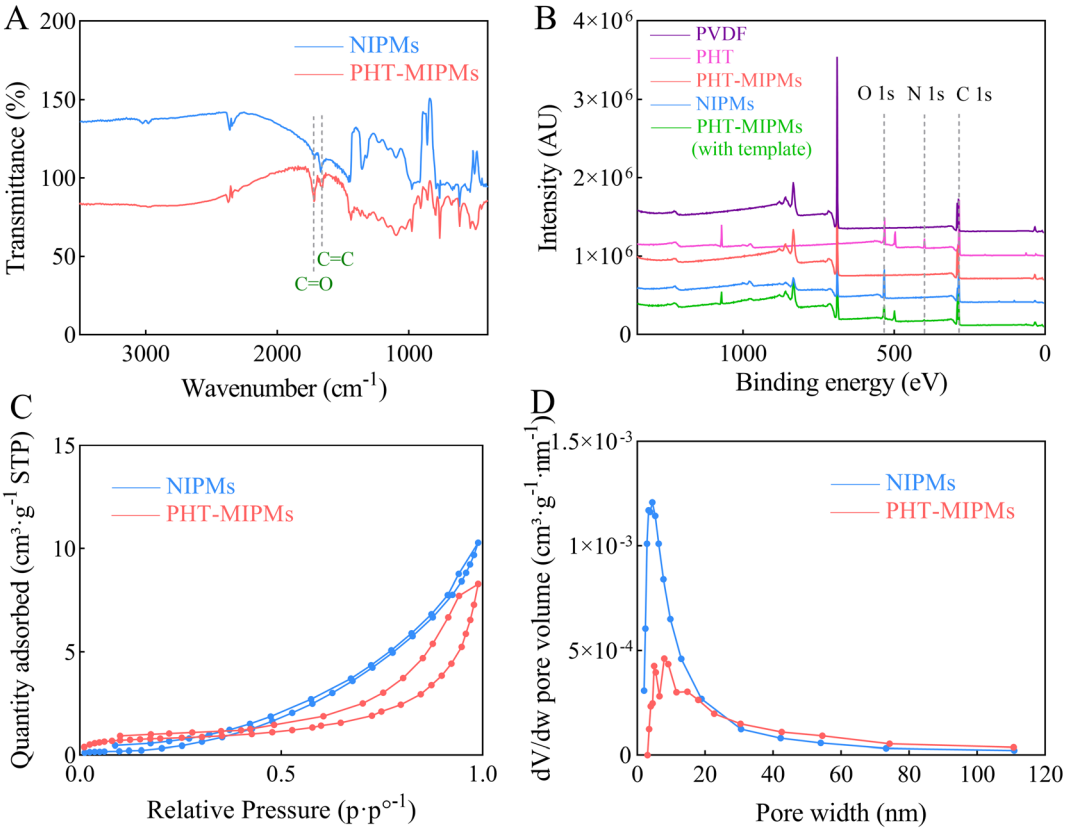

Fig. 3 FT-IR spectra (A), XPS summary spectra (B), nitrogen adsorption desorption isotherm curves (C), and pore size distribution curves (D) of PVDF, NIPMs, PHT, PHT-MIPMs or PHT-MIPMs with a template.

Table 1 BET analysis of PVDF, NIPMs and MIPMs

Membrane	Superficial area ($m^2\ g^{-1}$)	Pore volume ($cm^2\ g^{-1}$)	Pore size (nm)
NIPMs	0.9353	0.01591	8.11
MIPMs	3.006	0.01283	17.32

and LTG on MIPMs, which hinted that interactions may not exist between the adsorbed molecules, the transmigration of adsorbed molecules on the adsorption surface, and monolayer adsorption occurred at the binding sites with homogeneous energy levels. The dimensionless constant separation factor (R_L) was used to further predict the characteristics and feasibility of the Langmuir model. The formula for the calculation of R_L is $R_L = 1/(1 + bC_0)$, where b is the Langmuir model constant (mL μg^{-1}) and C_0 is the initial concentration ($\mu g\ mL^{-1}$). The results showed that the R_L values of PHT, PHB, and LTG were all distributed on a scale of 0 to 1, suggesting that a favorable process was present in the adsorption of PHT, PHB and LTG on MIPMs.[42]

The kinetic adsorption curves of MIPMs and NIPMs towards PHT, PHB, and LTG are presented in Fig. 5A–C, and the results showed that the adsorption capacities of MIPMs towards PHT, PHB, and LTG increased with an increase in time before 5 min, 20 min, and 20 min, respectively, followed by tending to flatten out. The experimental equilibrium adsorption capacities ($Q_{e(exp)}$) of MIPMs were 2.588, 2.241, and 2.275 mg g^{-1}, respectively. The adsorption capacities of NIPMs towards PHT, PHB, and LTG increased with an increase in time before 20 min, but were much lower than that of MIPMs. To explore the potential adsorption mechanism, the non-linear approach of pseudo-first-order and pseudo-second-order models was further used to fit the original data, and the results are shown in Fig. 5D–I and Table 3.[43–45] The correlation coefficients of PHT, PHB, and LTG from the pseudo-second-order kinetic models were all more than 0.999, which were higher than that in the pseudo-first-order kinetic model. The calculated equilibrium adsorption capacities ($Q_{e(cal)}$) of PHT, PHB, and LTG in the pseudo-second-order kinetic models were 2.612, 2.355, and 2.333 mg g^{-1}, respectively, which were higher and closer to the experimental adsorption capacities ($Q_{e(exp)}$) than that in pseudo-first-order kinetic models. Thus, these results suggest that the adsorption process of the target compounds on MIPMs may involve chemical interactions, and the adsorption rate may be influenced by the movement of the target molecules within the pores of MIPMs.

3.3.2. Adsorption selectivity. In this study, the structural analogue DPG and clinically possible co-administrated medicines including OXC and CBZ were used to investigate the adsorption selectivity of MIPMs and NIPMs, and the selectivity coefficients (α), relative selectivity coefficients (β), and

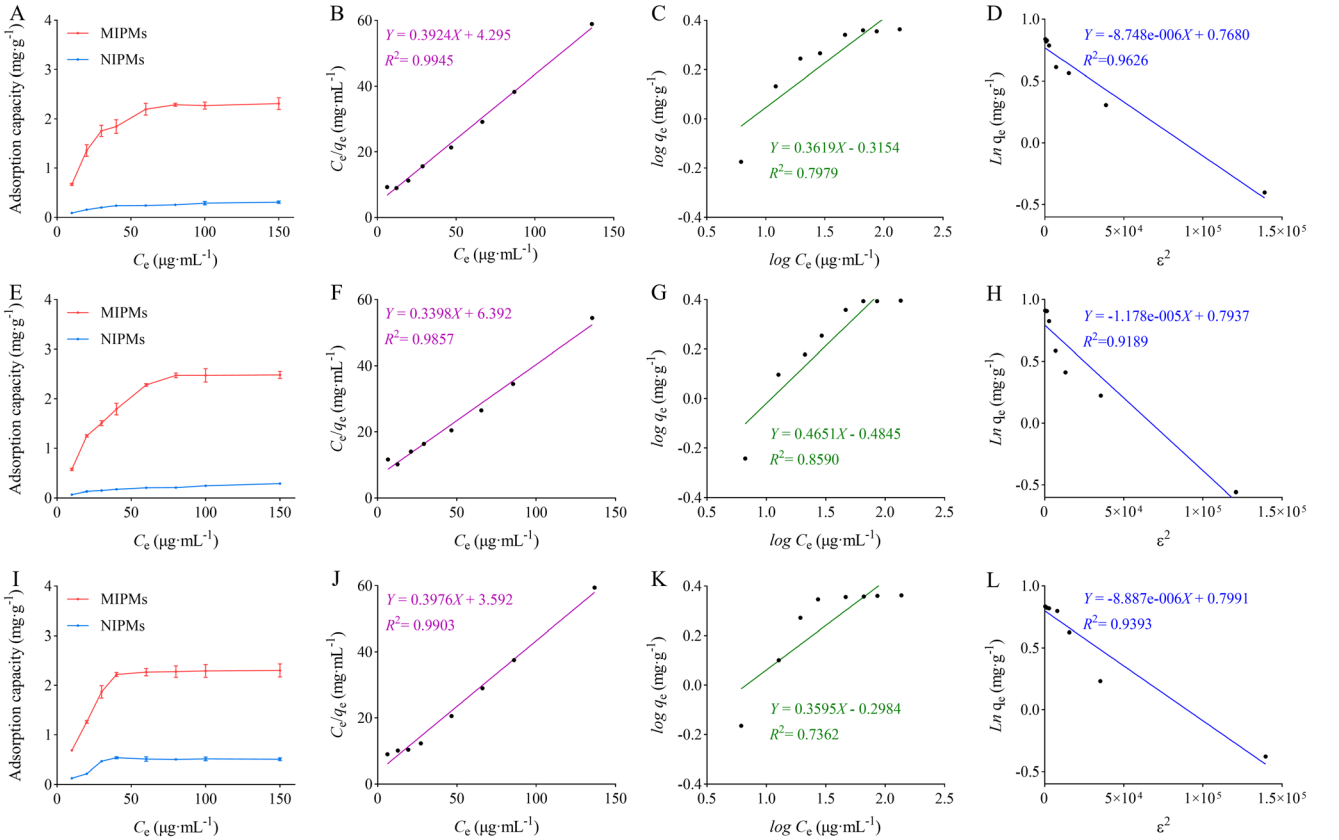

Fig. 4 Adsorption isotherm curves of MIPMs and NIPMs for PHT (A), PHB (E) and LTG (I) ($n = 3$) and illustration of the isotherm data presented in terms of the linearized Langmuir (B), (F) or (J), Freundlich (C), (G) or (K) and Dubinin–Radushkevich (D), (H) or (L) models. (B)–(D) represent the models of PHT. (F)–(H) represent the models of PHB. (J)–(L) represent the models of LTG.

imprinting factor (IF) were used to evaluate the selective performance of MIPMs or NIPMs towards PHT, PHB and LTG.30 As shown in Fig. S3,† the adsorption capacities of MIPMs towards the six compounds were found to be higher than that of NIPMs. Moreover, MIPMs presented better adsorption towards PHT, PHB, LTG, and DPG, but worse adsorption towards OXC and CBZ, which can be attributed to their similar structures. Consistent with the above-mentioned findings, the results in Table 4 show that the adsorption capacities of MIPMs towards PHT, PHB, LTG, DPG, OXC, and CBZ were obviously much higher than that of NIPMs. The selectivity adsorption coefficients (α) revealed that the adsorption capacities of MIPMs towards PHT, PHB, and LTG were 1.4-, 1.6-, 1.5-fold higher than that of DPG, 1.8-, 2.0-, 1.9-fold higher than that of OXC, and 2.3-, 2.5-, 2.3-fold higher than that of CBZ, respectively. In comparison, the adsorption capacities of NIPMs towards PHT, PHB, and LTG were 1.5-, 1.2-, 2.9-fold higher than that of DPG, 0.6-, 0.4-, 1.1-fold higher than that of OXC, and 0.6-, 0.4-, 1.1-fold higher than that of CBZ, respectively. These findings indicate that MIPMs presented better adsorption for PHT, PHB, and LTG and had significantly improved adsorption selectivity compared to NIPMs. The relative selectivity adsorption coefficients (β) indicated that the selective adsorption capabilities of MIPMs towards PHT or PHB against DPG were similar to that of NIPMs, while the selective adsorption capability of MIPMs for PHT/OXC, PHB/OXC, LTG/OXC, PHT/CBZ, PHB/CBZ, or LTG/CBZ was approximately 3.3-, 4.7-, 1.7-, 4.1-, 5.9-, or 2.2-fold higher than that of NIPMs, respectively.

The IF value is another important parameter that characterizes the specific recognition of MIPM, which was calculated

Table 2 Parameters of Langmuir, Freundlich and Dubinin–Radushkevich models for MIPMs towards PHT, PHB and LTG

	Langmuir			Freundlich			Dubinin–Radushkevich		
Analyte	Q_m (mg g^{-1})	K (mL μg^{-1})	R^2	n	K_F (mg g^{-1})	R^2	Q_m (mg g^{-1})	K_{ad} (mol^2 J^{-2})	R^2
PHT	2.548	0.09135	0.9945	2.763	0.4837	0.7979	2.155	−0.000009	0.9626
PHB	2.943	0.05316	0.9857	2.150	0.3277	0.8590	2.212	−0.00001	0.9189
LTG	2.515	0.1107	0.9903	3.351	0.4370	0.7362	2.224	−0.000009	0.9393

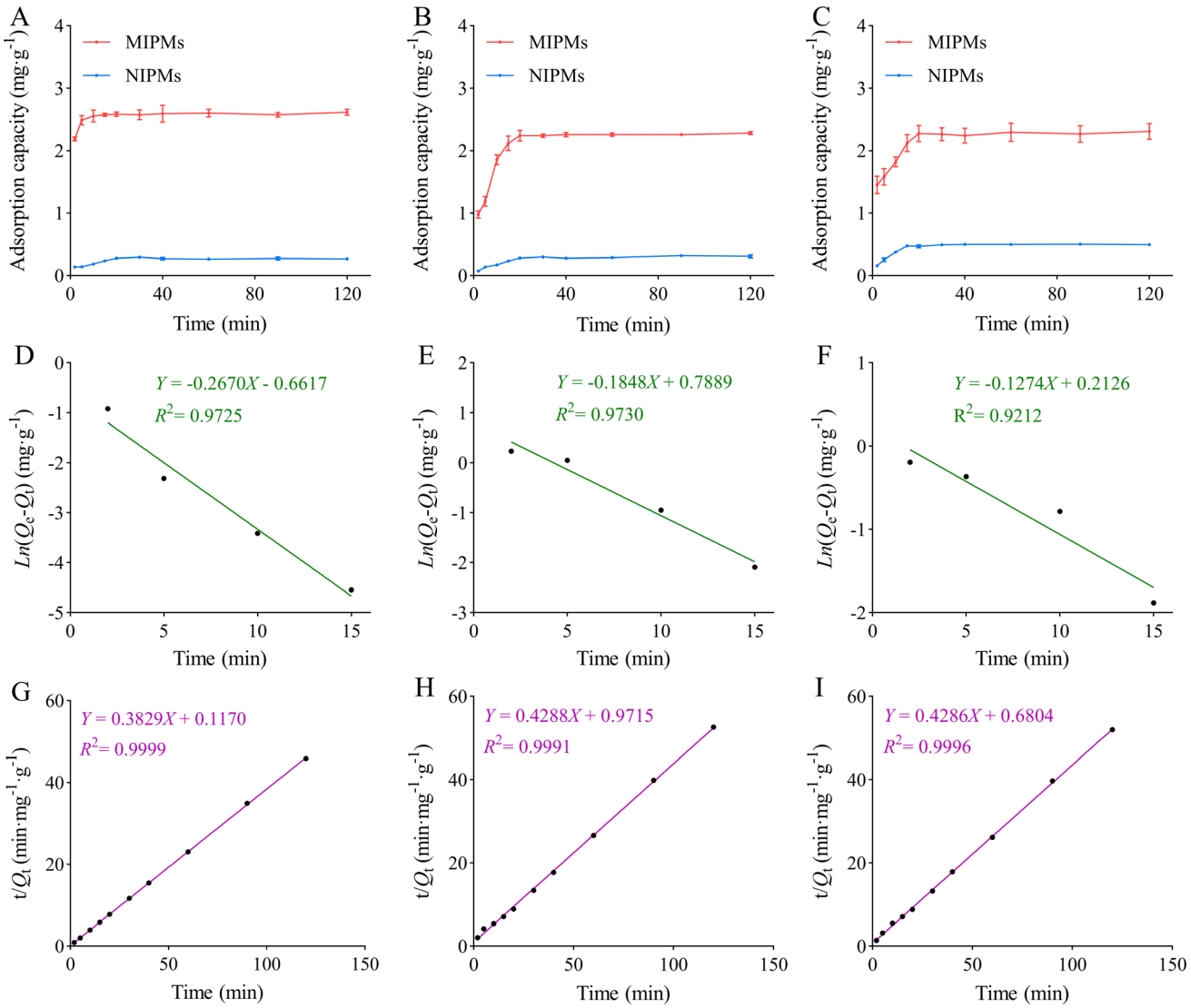

Fig. 5 Dynamic adsorption plots (A–C) ($n = 3$), pseudo-first-order (D–F) and pseudo-second-order (G–I) kinetic models for the adsorption of PHT, PHB or LTG by MIPMs.

by the ratio of adsorption capacity between MIPM and NIPM. Interestingly, our results showed that the IF value of the template PHT was not the highest but lower than that of PHB or DPG (Table 4), which may result from that similar recognition sites in the chemical structures of PHT, PHB and DPG, while the molecular size of PHB or DBG was lower than that of PHT. Moreover, the IF value of LTG was lower than that of PHT, PHB or DPG, which may be related to the high electronegativity of Cl in LTG, and thus result in LTG being easily adsorbed by NIPMs. Although the IF value of DPG was higher than that of PHT or LTG, the adsorption capacity (Q_e) of MIPM toward DPG was lower than that for PHT or LTG, and DPG was rarely presented in the experiment, which hinted that the usability of MIPMs in practical work may be reliable.

3.3.3. Optimization of adsorption–desorption. The eluent type and volume and the desorption time affected the

Table 3 Kinetic constants for the adsorption of PHT, PHB and LTG on MIPMs

		Pseudo-first-order kinetic model			Pseudo-second-order kinetic model		
Analyte	$Q_{e(exp)}$ (mg g^{-1})	$Q_{e(cal)}$ (mg g^{-1})	k_1	R^2	$Q_{e(cal)}$ (mg g^{-1})	k_2	R^2
PHT	2.588	1.938	0.6149	0.9725	2.612	0.06302	0.9999
PHB	2.241	2.201	0.4256	0.9730	2.355	0.1857	0.9991
LTG	2.275	1.136	0.4896	0.9212	2.333	0.07896	0.9996

Table 4 Parameters of adsorptive selectivity of MIPMs and NIPMs

	PHT-MIPMs				NIPMs							
Analyte	Q_e (mg g^{-1})	$\alpha_{(DPG)}$	$\alpha_{(OXC)}$	$\alpha_{(CBZ)}$	Q_e (mg g^{-1})	$\alpha_{(DPG)}$	$\alpha_{(OXC)}$	$\alpha_{(CBZ)}$	$\beta_{(DPG)}$	$\beta_{(OXC)}$	$\beta_{(CBZ)}$	IF
PHT	2.230	1.435	1.832	2.262	0.261	1.512	0.5612	0.5527	0.9492	3.264	4.093	8.538
PHB	2.462	1.611	2.057	2.540	0.203	1.171	0.4348	0.4282	1.376	4.731	5.932	12.122
LTG	2.288	1.484	1.895	2.340	0.502	2.948	1.094	1.078	0.5035	1.732	2.171	4.562
DPG	1.645	—	—	—	0.174	—	—	—	—	—	—	9.465
OXC	1.308	—	—	—	0.458	—	—	—	—	—	—	2.857
CBZ	1.086	—	—	—	0.464	—	—	—	—	—	—	2.342

desorption rates of PHT, PHB and LTG, which need to be investigated and optimized. As shown in Fig. S4–S6,† the desorption rates of PHT, PHB, and LTG adsorbed by MIPMs were the highest when methanol was used as the eluent, surpassing that of ACN, distilled water, and ethanol. Thus, methanol was chosen as the final desorption reagent. The desorption rate of PHT, PHB, and LTG reached the highest when the desorption time was 20 min, and was not obviously enhanced after 20 min. Thus, the desorption time was finally set at 20 min. In the case of the eluent volume, there was no notable difference in the desorption rate among different volumes of desorption reagents (methanol). However, considering factors such as environmental protection, safety and cost-effectiveness, it is preferable to use the minimum amount of desorption reagent. Therefore, the final desorption conditions of PHT, PHB and LTG on MIPMs were set as follows: 1 mL of methanol and desorption for 20 min.

3.3.4. Preparation reproducibility and reusability of MIPMs. The preparation reproducibility of MIPMs in the current study was investigated by evaluating the variation in adsorption capacity from 5 batches of MIPMs with three replicates. The results showed that the variation in adsorption capacity for PHT from the same batch of MIPMs was not more than 0.04%, while that of 5 batches of MIPMs was not greater than 3.48% (Table S10†). These results indicate that the preparation method of MIPMs in our current study is reproducible and reliable, which may result from the fact that the preparation of the PVDF membrane in this study was simple.

Reusability is another important aspect of polymers.[46] Thus, in our current study, the adsorption capacity of PHT, PHB and LTG on MIPMs was calculated after 8 adsorption–desorption cycles. As depicted in Fig. S7,† the variation in the adsorption capacity of PHT, PHB, and LTG on the same MIPMs was 13.88%, 13.92%, and 14.86% after 7 adsorption–resorption cycles, respectively, which demonstrated that the prepared MIPMs exhibited recyclability and could be utilized for at least 7 times.

3.4. Evaluation of application ability

To investigate the application of MIPMs for extracting PHT, PHB, and/or LTG from real samples, simulated samples were prepared and employed. The migration of the target molecules or the binding sites on the surface of MIPMs may be affected by endogenous macromolecular compounds found in biological samples, such as proteins, phospholipids, and DNA. Thus, to minimize the impact of these compounds on the extraction efficiency of MIPMs for the target compounds, in our study, we diluted the plasma using PBS, which closely resembles the body fluid of animals or humans. This was the first step in investigating the effects of diluting plasma with PBS on the extraction of the target compounds. As shown in Table S11,† the extraction recoveries of MIPMs for the 3 target analytes at a dilution ratio of 4 were significantly higher than that at the dilution ratio of 2. However, there was no obvious difference for extraction recoveries between the dilution ratio of 4 and 8. Therefore, PBS at a dilution ratio of 4 was used to dilute plasma before extraction using MIPMs.

The extraction recoveries of PHT, PHB and LTG from MIPMs in different matrices are listed in Table 5. The results showed that the extraction recoveries of MIPMs for PHT, PHB, or LTG in methanol, NS, and PBS were all greater than 80% with an RSD% value less than 3.64. The extraction recoveries of MIPMs for PHT and PHB in plasma were more than 80% with the RSD% value of less than 2.41 and that of MIPMs for LTG was more than 65% with the RSD% value of less than 0.99. These results indicate that MIPMs can be used to extract PHT, PHB, and LTG in different real matrices, such as organic solution, environmental water, urine, and plasma.

Moreover, the analytical performance of the prepared MIPMs for the extraction of PHT and PHB from plasma was compared to that of ACN protein precipitation from the aspects of extraction recovery and anti-interferences of endogenous compounds. As illustrated in Fig. S8, S9 and Table S12,† the extraction recovery of MIPMs for PHT was obviously higher than that of ACN protein precipitation; however, the extraction recoveries of both methods were all more than 80% with RSD% less than 4.14%. For the extraction recovery of PHB, there was no significant difference between both methods. Moreover, MIPM treatment could obviously reduce the interferences from endogenous compounds in the extraction of PHT and PHB compared with ACN protein precipitation. Furthermore, the proposed method was compared with some other available methods based on MIPs or membrane extraction in the literature for PHT, PHB, and/or LTG.[28–33,47–53] As shown in Table 6, the extraction recovery of the current method for PHT in plasma was similar with that in the works by Jia's group[28] and Yaripour's group[33] but higher than that in other methods.[47,48,53] The extraction recovery of the current work for PHT in aqueous solution was obviously higher than that in the reference

Table 5 Extraction recovery of MIPMs towards OXC, CBZ, MHD, and CBZE in different matrices ($n = 5$)[a]

		Recovery (%)							
		Matrix							
		Methanol		NS		PBS		Plasma	
Analyte	Nominal concentration (μg mL^{-1})	Mean ± SD	RSD%	Mean ± SD	RSD%	Mean ± SD	RSD%	Mean ± SD	RSD%
PHT	3.16	85.52 ± 1.46	1.71	85.68 ± 0.87	1.01	96.01 ± 0.82	0.86	88.47 ± 2.13	2.41
	12.63	87.25 ± 1.81	2.08	85.89 ± 1.04	1.22	95.99 ± 1.31	1.37	87.38 ± 1.45	1.66
	42.08	86.70 ± 1.96	2.26	84.09 ± 1.18	1.41	95.89 ± 1.43	1.49	90.62 ± 0.76	0.84
PHB	2.95	83.56 ± 0.88	1.06	82.65 ± 2.19	2.65	91.87 ± 3.34	3.64	82.67 ± 0.95	1.15
	11.81	86.49 ± 2.74	3.17	82.38 ± 2.33	2.83	90.59 ± 2.42	2.67	83.57 ± 1.37	1.64
	39.37	85.64 ± 2.16	2.52	82.54 ± 0.99	1.20	92.84 ± 2.64	2.84	84.28 ± 1.03	1.22
LTG	6.36	80.15 ± 1.01	1.26	80.25 ± 0.59	0.74	83.98 ± 2.49	2.97	65.38 ± 0.65	0.99
	25.44	81.22 ± 2.33	2.87	80.43 ± 1.72	2.14	84.92 ± 1.06	1.25	67.23 ± 0.42	0.62
	63.60	84.11 ± 0.64	0.76	81.80 ± 0.38	0.47	84.93 ± 0.78	0.91	69.26 ± 0.34	0.49

[a] NS, normal saline; PBS, phosphate buffer solution.

methods.[47,52] In the case of PHB, the extraction recovery in the current work for plasma was higher than that of the reported methods,[50,53] while the extraction recovery in current work for aqueous solution was higher than that of MIPs or electromembrane extraction[49,52,53] but similar with that of MIP fiber extraction,[29] which may result from the similar characters between MIP fiber and MIPMs. In the case of LTG, the extraction recovery of the employed method for plasma or aqueous solution was lower than that of previous works based on MIPs,[30–32,51] which may result from the different templates used to prepare the MIPs.

Table 6 Comparison of the results with other methods for PHT, PHB, and LTG based on MIPs or membrane extraction[a]

Extraction method	Analyte	Matrix	Extraction recovery	Analytical method	Ref.
MIPs extraction	PHT	Plasma	89.2–94.3%	HPLC-UV	28
MIPs extraction	PHT	Wastewater, plasma, and urine	77.0%, 42.0%, and 43.0%	HPLC-UV	47
MIPs extraction	PHT	Plasma	58.0–78.0%	HPLC-UV	48
MIPs fiber extraction	PHB	Urine	94.3–98.5%	HPLC-UV	29
MIPs extraction	PHB	Urine	81.0–86.0%	HPLC-UV	49
MIPs extraction	PHB	Plasma	75.0%	HPLC-UV	50
MMIPs extraction	LTG	Serum	76.6–79.0%	HPLC-UV	30
MMIPs extraction	LTG	Urine	97.1–98.0%	HPLC-UV	31
		Plasma	96.6%-97.0		
MIPs extraction	LTG	Serum	80.8–83.8%	HPLC-UV	32
MIPs extraction	LTG	Serum	84.0–89.0%	HPLC-UV	51
Electromembrane extraction	PHT	Plasma and urine	88.0–92.0%	HPLC-UV	33
Electromembrane extraction	PHT	Water solution	42.2%	HPLC-UV	52
	PHB		33.0%		
Electromembrane extraction	PHT	Plasma, saliva, and urine	20.6%	HPLC-UV	53
	PHB		11.7%		
MIPMs extraction	PHT	Methanol	85.5–87.3%	HPLC-UV	This work
		NS	84.1–85.9%		
		PBS	95.9–96.0%		
		Plasma	87.4–90.6%		
	PHB	Methanol	83.6–86.5%		
		NS	82.4–82.7%		
		PBS	90.6–92.8%		
		Plasma	82.7–84.3%		
	LTG	Methanol	80.2–84.1%		
		NS	80.3–81.8%		
		PBS	84.0–84.9%		
		Plasma	65.4–69.3%		

[a] MIPs: molecularly imprinted polymers; MMIPs: magnetic molecularly imprinted polymers; MIPMs: molecularly imprinted polymer membranes.

4. Conclusion

In the current study, an innovative MIPM was prepared with PVDF as the support and PHT as the single template, which could simultaneously be adapted to extract and separate PHT, PHB and LTG in different matrices including methanol, NS, PBS and plasma. This preparation method involved simple methanol activation of the supporting membrane without complicated chemical modification and one-step initiation polymerization and grafting of the molecularly imprinted polymer, and thus was simple, easy and rapid. According to the series of characterization, MIPMs presented excellent adsorption performances, reproducibility, and reusability. The maximum adsorption capacity of the MIPMs towards PHT, PHB and LTG was 2.312, 2.485, and 2.303 mg g^{-1}, respectively, and their adsorption behaviors followed the pseudo-second-order kinetic equation. The prepared MIPMs exhibited extraction recoveries of over 80% for PHT, PHB, and LTG in methanol, NS, and PBS, as well as for PHT and PHB in plasma. In addition, MIPM treatment could obviously decrease the interferences from endogenous compounds in plasma. All the above-mentioned results suggested that the synthesized MIPMs can be used to extract PHT, PHB, and LTG in real organic solution, environmental water and urine, and PHT and PHB in real plasma. Taken together, our study successfully prepared new MIPMs that offered alternative selectivity for the extraction of PHT, PHB, and/or LTG in different matrices, which presented promising potential for application in real organic solutions in the chemical industry, environment water, urine and plasma.

Author contributions

Conceptualization, Dao-quan Tang; methodology, Yan-lin Zhao, Yu-xin You, and Yu-lang Chen; software, Yu-lang Chen and Ying Zhang; validation, Yan-lin Zhao and Yu-xin You; investigation, Yan-lin Zhao, Yu-xin You, Yu-lang Chen, and Ying Zhang; resources, Yan-lin Zhao; data curation, Yan-lin Zhao, Yu-xin You, and Yu-lang Chen; writing-original draft preparation, Yan-lin Zhao; writing-review and editing, Dao-quan Tang; supervision, Yan Du and Dao-quan Tang; project administration, Yan Du and Yan-lin Zhao. All authors have read and agreed to the published version of the article.

Conflicts of interest

The authors declare that they have no known competing financial interests or personal relationships that could have appeared to influence the work reported in this paper.

Acknowledgements

This work was supported by the Natural Science Foundation of Jiangsu Province (No. BK20181147 and BE2019640), Natural Science Foundation of Xuzhou City of China (No. KC23334), and the Natural Science Foundation of Suining County of Jiangsu Province (No. SN202208).

References

1 S. Garcia-Rosa, B. de Freitas Brenha, V. F. da Rocha, E. Goulart and B. H. Silva Araujo, Personalized medicine using cutting edge technologies for genetic epilepsies, *Curr. Neuropharmacol.*, 2021, **19**, 813–831.
2 D. Ding, D. Zhou, J. W. Sander, W. Wang, S. Li and Z. Hong, Epilepsy in China: major progress in the past two decades, *Lancet Neurol.*, 2021, **20**, 316–326.
3 C. Johannessen Landmark, S. I. Johannessen and P. N. Patsalos, Therapeutic drug monitoring of antiepileptic drugs: current status and future prospects, *Expert Opin. Drug Metab. Toxicol.*, 2020, **16**, 227–238.
4 G. Liparoti, B. Burchiani, E. Mencaroni, D. Tripodi, G. Di Cara and A. Verrotti, Individualizing doses of antiepileptic drugs, *Expert Opin. Drug Metab. Toxicol.*, 2022, **18**, 219–233.
5 S. R. Mathews, D. K. Badyal and R. Mathew, Phenytoin-induced bradycardia and hypotension, *Indian J. Pharmacol.*, 2019, **51**, 120–122.
6 G. Gyandeep, S. S. Behura, S. K. Sahu and S. K. Panda, Comparison between Phenobarbitone and Levetiracetam as the initial anticonvulsant in preterm neonatal seizures – a pilot randomized control trial in developing country setup, *Eur. J. Pediatr.*, 2023, **182**, 2133–2138.
7 L. Bättig, C. Dünner, D. Cserpan, A. Rüegger, C. Hagmann, B. Schmitt, F. Pisani and G. Ramantani, Levetiracetam *versus* phenobarbital for neonatal seizures: a retrospective cohort study, *Pediatr. Neurol.*, 2023, **138**, 62–70.
8 J. He, X. Wu and D. Zhou, The efficacy of lamotrigine after failure of the first administration of valproate in treating epilepsy: a systematic review and meta-analysis, *Ann. Palliat. Med.*, 2022, **11**, 113–122.
9 A. N. Edinoff, L. H. Nguyen, M. J. Fitz-Gerald, E. Crane, K. Lewis, S. S. Pierre, A. D. Kaye, A. M. Kaye, J. S. Kaye, R. J. Kaye, S. A. Gennuso, G. Varrassi, O. Viswanath and I. Urits, Lamotrigine and Stevens-Johnson Syndrome prevention, *Psychopharmacol. Bull.*, 2021, **51**, 96–114.
10 B. Alyahya, M. Friesen, B. Nauche and M. Laliberté, Acute lamotrigine overdose: a systematic review of published adult and pediatric cases, *Clin. Toxicol.*, 2018, **56**, 81–89.
11 O. Golovko, A. L. Rehrl, S. Köhler and L. Ahrens, Organic micropollutants in water and sediment from Lake Mälaren, Sweden, *Chemosphere*, 2020, **258**, 127293.
12 N. H. Tran, M. Reinhard and K. Y. Gin, Occurrence and fate of emerging contaminants in municipal wastewater treatment plants from different geographical regions – a review, *Water Res.*, 2018, **133**, 182–207.
13 T. P. Wood, C. Du Preez, A. Steenkamp, C. Duvenage and E. R. Rohwer, Database-driven screening of South African surface water and the targeted detection of pharmaceuticals using liquid chromatography – high resolution mass spectrometry, *Environ. Pollut.*, 2017, **230**, 453–462.
14 I. Ferrer and E. M. Thurman, Identification of a new antidepressant and its glucuronide metabolite in water

samples using liquid chromatography/quadrupole time-of-flight mass spectrometry, *Anal. Chem.*, 2010, **82**, 8161–8168.

15 J. D. Cardoso-Vera, L. M. Gómez-Oliván, H. Islas-Flores, S. García-Medina, J. M. Orozco-Hernández, G. Heredia-García, G. A. Elizalde-Velázquez, M. Galar-Martínez and N. SanJuan-Reyes, Acute exposure to environmentally relevant concentrations of phenytoin damages early development and induces oxidative stress in zebrafish embryos, *Comp. Biochem. Physiol., Part C: Toxicol. Pharmacol.*, 2022, **253**, 109265.

16 J. D. Cardoso-Vera, L. M. Gómez-Oliván, H. Islas-Flores, S. García-Medina, G. A. Elizalde-Velázquez, J. M. Orozco-Hernández, G. Heredia-García, K. E. Rosales-Pérez and M. Galar-Martínez, Multi-biomarker approach to evaluate the neurotoxic effects of environmentally relevant concentrations of phenytoin on adult zebrafish *Danio rerio*, *Sci. Total Environ.*, 2022, **834**, 155359.

17 R. Gorovits, I. Sobol, K. Akama, B. Chefetz and H. Czosnek, Pharmaceuticals in treated wastewater induce a stress response in tomato plants, *Sci. Rep.*, 2020, **10**, 1856.

18 F. B. Nunes, F. da Silva Bruckmann, T. da Rosa Salles and C. R. B. Rhoden, Study of phenobarbital removal from the aqueous solutions employing magnetite-functionalized chitosan, *Environ. Sci. Pollut. Res. Int.*, 2023, **30**, 12658–12671.

19 A. Lajeunesse, C. Gagnon, F. Gagné, S. Louis, P. Cejka and S. Sauvé, Distribution of antidepressants and their metabolites in brook trout exposed to municipal wastewaters before and after ozone treatment – evidence of biological effects, *Chemosphere*, 2011, **83**, 564–571.

20 M. Sörengård, H. Campos-Pereira, M. Ullberg, F. Y. Lai, O. Golovko and L. Ahrens, Mass loads, source apportionment, and risk estimation of organic micropollutants from hospital and municipal wastewater in recipient catchments, *Chemosphere*, 2019, **234**, 931–941.

21 M. Goldstein, T. Malchi, M. Shenker and B. Chefetz, Pharmacokinetics in plants: carbamazepine and its interactions with lamotrigine, *Environ. Sci. Technol.*, 2018, **52**, 6957–6964.

22 S. Golbaz, M. Zamanzadeh, K. Yaghmaeian, R. Nabizadeh, N. Rastkari and H. Esfahani, Occurrence and removal of psychiatric pharmaceuticals in the Tehran South Municipal Wastewater Treatment Plant, *Environ. Sci. Pollut. Res. Int.*, 2023, **30**, 27041–27055.

23 Y. L. Zhao, L. L. Zhao, Y. X. You, X. X. Zheng, Y. Du and D. Q. Tang, Development and evaluation of a simple and easy high-performance liquid chromatography-ultraviolet system simultaneously suitable for determination of 24 anti-epileptic drugs in plasma, *J. Sep. Sci.*, 2022, **45**, 2161–2176.

24 D. S. Villarreal-Lucio, K. X. Vargas-Berrones, L. Díaz de León-Martínez and R. Flores-Ramíez, Molecularly imprinted polymers for environmental adsorption applications, *Environ. Sci. Pollut. Res. Int.*, 2022, **29**, 89923–89942.

25 M. R. Gama and C. B. Bottoli, Molecularly imprinted polymers for bioanalytical sample preparation, *J. Chromatogr. B: Anal. Technol. Biomed. Life Sci.*, 2017, **1043**, 107–121.

26 T. Hu, R. Chen, Q. Wang, C. He and S. Liu, Recent advances and applications of molecularly imprinted polymers in solid-phase extraction for real sample analysis, *J. Sep. Sci.*, 2021, **44**, 274–309.

27 K. Hoshina, S. Horiyama, H. Matsunaga and J. Haginaka, Molecularly imprinted polymers for simultaneous determination of antiepileptics in river water samples by liquid chromatography-tandem mass spectrometry, *J. Chromatogr. A*, 2009, **1216**, 4957–4962.

28 M. Jia, Y. Zhu, D. Guo, X. Bi and X. Hou, Surface molecularly imprinted polymer based on core-shell Fe_3O_4@MIL-101(Cr) for selective extraction of phenytoin sodium in plasma, *Anal. Chim. Acta*, 2020, **1128**, 211–220.

29 M. Rahimi and S. Bahar, Preparation of a new solid-phase microextraction fiber based on molecularly imprinted polymers for monitoring of phenobarbital in urine samples, *J. Chromatogr. Sci.*, 2022, **61**, 87–95.

30 Y. Q. Wei, L. L. Zhao, Y. X. You, Y. L. Zhao, X. X. Zheng, Y. Du and D. Q. Tang, Development of magnetic molecularly imprinted polymers with double templates for the rapid and selective determination of carbamazepine and lamotrigine in serum, *RSC Adv.*, 2022, **12**, 10051–10061.

31 M. Behbahani, S. Bagheri, M. M. Amini, H. Sadeghi Abandansari, H. Reza Moazami and A. Bagheri, Application of a magnetic molecularly imprinted polymer for the selective extraction and trace detection of lamotrigine in urine and plasma samples, *J. Sep. Sci.*, 2014, **37**, 1610–1616.

32 D. Y. Yin, N. Lyu, Z. T. Qian, L. L. Zhao, L. Wang, D. Q. Tang and Y. Du, Synthesis of molecularly imprinted polymers based on a new monomer "2-(4-vinylphenyl) quinoline-4-carboxylic acid" for the selective solid-phase extraction of lamotrigine, *J. Chromatogr. Sci.*, 2023, **61**, 195–202.

33 S. Yaripour, S. Nojavan, M. R. Khoshayand and A. Mohammadi, Electromembrane extraction of phenytoin from biological fluids: a survey on the effects of molecularly imprinted polymer and carbon nanotubes on extraction efficiency, *Microchem. J.*, 2020, **156**, 104800.

34 H. Yu, R. Yao and S. Shen, Development of a novel assay of molecularly imprinted membrane by design-based Gaussian pattern for vancomycin determination, *J. Pharm. Biomed. Anal.*, 2019, **175**, 112789.

35 S. Ncube, N. Tavengwa, A. Soqaka, E. Cukrowska and L. Chimuka, Development of a single format membrane assisted solvent extraction-molecularly imprinted polymer technique for extraction of polycyclic aromatic hydrocarbons in wastewater followed by gas chromatography mass spectrometry determination, *J. Chromatogr. A*, 2018, **1569**, 36–43.

36 Y. Yuan, X. Yuan, Q. Hang, R. Zheng, L. Lin, L. Zhao and Z. Xiong, Dummy molecularly imprinted membranes based on an eco-friendly synthesis approach for recognition and extraction of enrofloxacin and ciprofloxacin in egg samples, *J. Chromatogr. A*, 2021, **1653**, 462411.

37 X. Qiu, X. Y. Xu, Y. Liang, Y. Hua and H. Guo, Fabrication of a molecularly imprinted polymer immobilized membrane with nanopores and its application in determination of β_2-agonists in pork samples, *J. Chromatogr. A*, 2016, **1429**, 79–85.

38 I. Pereira, M. F. Rodrigues, A. R. Chaves and B. G. Vaz, Molecularly imprinted polymer (MIP) membrane assisted direct spray ionization mass spectrometry for agrochemicals screening in foodstuffs, *Talanta*, 2018, **178**, 507–514.

39 J. Wang and X. Guo, Adsorption isotherm models: Classification, physical meaning, application and solving method, *Chemosphere*, 2020, **258**, 127279.

40 D. Liu, R. Zhao, S. Zhao, Z. Wang, R. Liu, F. Wang and Y. Gao, A developed HPLC-MS/MS method to quantitate 5 steroid hormones in clinical human serum by using PBS as the surrogate matrix, *J. Chromatogr. B: Anal. Technol. Biomed. Life Sci.*, 2021, **1186**, 123002.

41 S. Ongay, G. Hendriks, J. Hermans, M. van den Berge, N. H. ten Hacken, N. C. van de Merbel and R. Bischoff, Quantification of free and total desmosine and isodesmosine in human urine by liquid chromatography tandem mass spectrometry: a comparison of the surrogate-analyte and the surrogate-matrix approach for quantitation, *J. Chromatogr. A*, 2014, **1326**, 13–19.

42 E. E. Abdel-Hady, H. F. M. Mohamed, S. H. M. Hafez, A. M. M. Fahmy, A. Magdy, A. S. Mohamed, E. O. Ali, H. R. Abdelhamed and O. M. Mahmoud, Textural properties and adsorption behavior of Zn-Mg-Al layered double hydroxide upon crystal violet dye removal as a low cost, effective, and recyclable adsorbent, *Sci. Rep.*, 2023, **13**, 6435.

43 M. Hayat, S. Manzoor, N. Raza, A. Abbas, M. I. Khan, N. Elboughdiri, K. Naseem, A. Shanableh, A. M. M. Elbadry, S. Al Arni, M. Benaissa and F. A. Ibrahim, Molecularly imprinted polymeric sorbent for targeted dispersive solid-phase microextraction of fipronil from milk samples, *ACS Omega*, 2022, **7**, 41437–41448.

44 D. Karadag, Y. Koc, M. Turan and M. Ozturk, A comparative study of linear and non-linear regression analysis for ammonium exchange by clinoptilolite zeolite, *J. Hazard. Mater.*, 2007, **144**, 432–437.

45 F. Galvanin, M. Barolo, S. Macchietto and F. Bezzo, Optimal design of clinical tests for the identification of physiological models of type 1 diabetes in the presence of model mismatch, *Med. Biol. Eng. Comput.*, 2011, **49**, 263–277.

46 J. Kupai, M. Razali, S. Buyuktiryaki, R. Kecili and G. Szekely, Long-term stability and reusability of molecularly imprinted polymers, *Polym. Chem.*, 2017, **8**, 666–673.

47 E. Abdollahi, M. Abdouss and A. Mohammadi, Synthesis of a nano molecularly imprinted polymeric sorbent for solid phase extraction and determination of phenytoin in plasma, urine, and wastewater by HPLC, *RSC Adv.*, 2016, **6**, 39095.

48 A. Bereczki, A. Tolokán, G. Horvaia, V. Horváth, F. Lanza, A. J. Hall and B. Sellergren, Determination of phenytoin in plasma by molecularly imprinted solid-phase extraction, *J. Chromatogr. A*, 2001, **930**, 31–38.

49 S. G. Hu, S. W. Wang and X. W. He, An amobarbital molecularly imprinted microsphere for selective solid-phase extraction of phenobarbital from human urine and medicines and their determination by high-performance liquid chromatography, *Analyst*, 2003, **128**, 1485–1489.

50 E. J. Pilau, R. G. C. Silva, I. C. F. S. Jardim and F. Augusto, Molecularly imprinted sol-gel silica for solid phase extraction of phenobarbital, *J. Braz. Chem. Soc.*, 2008, **19**, 1136–1143.

51 S. A. Mohajeri and S. A. Ebrahimi, Preparation and characterization of a lamotrigine imprinted polymer and its application for drug assay in human serum, *J. Sep. Sci.*, 2008, **31**, 3595–3602.

52 R. Dolatabadi, A. Mohammadi and R. B. Walker, A novel three-dimensional printed device with conductive elements for electromembrane extraction combined with high-performance liquid chromatography and ultraviolet detector, *J. Sep. Sci.*, 2022, **45**, 3187–3196.

53 R. Dolatabadi, A. Mohammadi, S. Nojavan, S. Yaripour, A. Tafakhori and M. Shirangi, Electromembrane extraction-high-performance liquid chromatography-ultraviolet detection of phenobarbital and phenytoin in human plasma, saliva, and urine, *J. Chin. Chem. Soc.*, 2021, **68**, 1522–1530.